Precision Motion Control With Disturbance Observer for Pulsewidth-Modulated-Driven Permanent-Magnet Linear Motors

Kok Kiong Tan, Tong Heng Lee, Hui Fang Dou, Shok Jun Chin, and Shao Zhao

***Abstract*—In this paper, we address the problem of precision motion control of permanent-magnet linear motors (PMLMs) under the influence of significant disturbances. We establish a mathematical model of a PMLM driven by a sinusoidal pulsewidth-modulated (PWM) amplifier, obtaining it from a describing function analysis of the essentially nonlinear characteristics. The overall model (PWM+PMLM) inevitably inherits uncertainties in the face of load changes, system parameter perturbation, noise, and inherent system nonlinearities, etc., all of which constitute disturbances to the control system that will adversely affect the precision and accuracy. We propose a robust control scheme employing a disturbance observer to address the sensitivity of the control performance to the disturbances. Real-time experimental results are provided to verify and confirm the practical effectiveness of the proposed approach.**

***Index Terms*—Disturbance observer, precision motion control, PWM amplifier.**

I. Introduction

EVER-INCREASING demands on higher productivity and better product quality in advanced manufacturing industries, such as the semiconductor and precision engineering industries, has continued to motivate and stimulate the development of high-speed and high-precision motion control systems. Among the various electric motor drives, permanent-magnet linear motors (PMLMs) are probably the most naturally akin to applications requiring high speed and high precision. The main features of a PMLM include high force density achievable, low thermal losses, high dynamic performance, and probably most importantly, the high positioning precision and accuracy associated with the mechanical simplicity. Unlike rotary machines, linear motors require no indirect coupling mechanisms as in gear boxes, chains, and screw coupling. This greatly reduces the effects of contact-types of nonlinearities and disturbances such as backlash and frictional forces [1].

However, the achievable performance of PMLMs is unavoidably limited by the amount of disturbances present. These disturbances may arise due to load changes, system parameter perturbation owing to prolonged usage, measurement noise and high frequencies generated from the amplifiers (especially when a pulsewidth-modulated (PWM) amplifier is used), or inherent nonlinear dynamics. For the PMLM, a significant nonlinear phenomenon is due to the force ripple effect, which arises from the magnetic structure and exhibits position-dependent characteristics. Due to the direct-drive principle behind the operation of a linear motor, this parasitic force ripple has significant effects on the position accuracy achievable and it may also cause oscillations and yield stability problems, particularly at low velocities or with a light load (low momentum). This is a prominent factor limiting the performance of PMLMs [2]. To achieve high-speed and high-precision motion control, the force ripple effects cannot be undermined and they should be suppressed. Other nonlinear forces at work include the various forms of motion impeding frictional forces.

Due to the typical precision positioning requirements and low offset tolerance of their applications, the control of PMLMs under the influence of disturbances is particularly challenging since conventional proportional–integral–derivative (PID) control usually may not suffice in these application domains. Some efforts have been made toward more advanced control of PMLM motion systems. In [3], a neural-network (NN) based feedforward assisted feedback controller was proposed. A hybrid control strategy using a variable structure control (VSC) is suggested for submicron positioning control [4]. Tan *et al.* [5] proposed an artificial relay tuning and zero-phase filtering-based iterative learning control (ILC) for high-precision motion control.

In this paper, we are focused on an industrial grade PMLM manufactured by Linear Drive Ltd., although the results to be presented are generally applicable to other systems. Previous works ([6] and [7]) on this system have shown that the inherent force ripples as well as the high-frequency harmonics arising from the PWM amplifier are the major disturbance sources which can seriously degrade the positioning accuracy achievable by the control system. Incorporating a higher resolution in the measurement system via the use of high interpolation electronics on the encoder signals can only achieve improvement in positioning accuracy to a limited extent. Thereafter, the amount of disturbances present will ultimately determine the achievable performance. In this paper, we attempt to address this important issue of disturbance compensation for precision motion control systems.

First, based on a describing function approach [8], we will establish an overall model for a dc PMLM driven by a sinusoidal PWM amplifier. For practical control design purposes, the desirable system model to be applied is usually a linear one. In this paper, the amplifier model used is a first-order quasi-linear approximation, considering only the fundamental frequency of the

Manuscript received August 24, 2000; revised February 4, 2003.

The authors are with the Department of Electrical Engineering, National University of Singapore, 117576 Singapore (e-mail: kktan@nus.edu.sg; eleleeth@nus.edu.sg; eledouhf@nus.edu.sg; engp8888@nus.edu.sg; engp1564@nus.edu.sg).

Digital Object Identifier 10.1109/TMAG.2003.810617

multitude of frequencies generated by the amplifier. The PMLM model is a third-order transfer function.

Therefore, the overall mathematical model will inevitably inherit modeling uncertainties, and a robust control scheme is thus necessary. In this paper, one such scheme is proposed which augments a disturbance observation/cancellation scheme [9] to the motion controller to reduce the sensitivity of the control performance to disturbances arising. The control and disturbance compensator design is relatively simple and directly amenable to practical applications. This practical viability is a major concern of this paper. Therefore, full experimental results are documented to illustrate the effectiveness of the proposed robust control system for PMLM precision motion control.

II. System Descriptions

A. Permanent-Magnet Linear Motor

The dynamics of a PMLM can be described by

$$u(t) = k_e\dot{x}(t) + Ri_q(t) + L\frac{di_q(t)}{dt} \tag{1}$$

$$f(t) = k_f i_q(t) \tag{2}$$

$$f(t) = m\ddot{x}(t) + f_{\text{load}}(t) + f_{\text{fric}}(t) + f_{\text{ripple}}(\dot{x}, x) + f_n(t) \tag{3}$$

where $u(t)$ and $i_q(t)$ are the time-varying motor terminal voltage and the equivalent armature current, respectively; $x(t)$ is the motor position; $f(t)$ and $f_{\text{load}}(t)$ are the developed force and the applied load force, respectively; and $f_{\text{fric}}(t)$ and $f_{\text{ripple}}(t)$ denote the frictional and ripple forces, respectively. The term $f_n(t)$ includes other residual uncertainties and disturbances in the system. The notations of other physical parameters are clearly documented in [10].

As mentioned, the force ripple constitutes one significant source of disturbances for PMLM based motion control systems. The two primary sources of force ripple, f_{ripple}, are the cogging (or detent) force and the reluctance force. The cogging force arises as a result of the mutual attraction between the magnets and iron cores of the translator. This force exists even in the absence of any winding current and it exhibits a periodic relationship with respect to the position of the translator relative to the magnets. Cogging manifests itself by the tendency of the translator to align in a number of preferred position regardless of excitation states. There are two potential causes of the periodic cogging force in PMLMs, resulting from the slotting and the finite length of iron-core translator. The reluctance force is due to the variation of the self-inductance of the windings with respect to the relative position between the translator and the magnets. Thus, the reluctance force also has a periodic relationship with the translator-magnet position. Collectively, the cogging and reluctant force constitute the overall force ripple phenomenon.

Fig. 1 shows the velocity-position characteristics of a tubular-type PMLM manufactured by Linear Drive (U.K.) with different step sizes (i.e., different steady-state velocities). Interesting observations may be inferred from these responses. First, the ripple period is independent of the step size (i.e., independent of the velocity), but it has a fixed relationship with respect to position. Second, the ripple amplitude is dependent on both position and velocity. At a higher velocity, the ripple amplitude decreases compared to when the motor is run at a lower velocity where the full dosage of ripple effects is experienced.

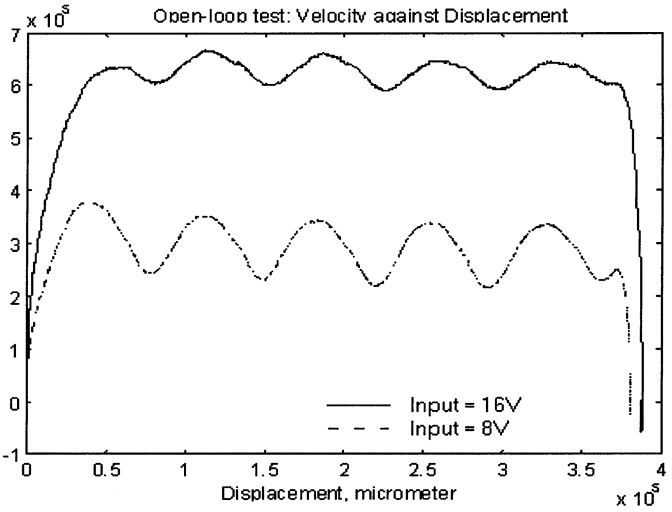

Fig. 1. Velocity (μm/s) against position (μm) for different step voltages.

Neglecting all the nonlinearities and uncertainties in (3), the dynamics of PMLM can be reduced to

$$u(t) = k_e\dot{x}(t) + \frac{mR}{k_f}\ddot{x}(t) + \frac{mL}{k_f}\dddot{x}(t). \tag{4}$$

The transfer function from input voltage to velocity is essentially of second order. In fact, the second-order model has been found to be widely adequate for many industrial applications encountered. The dominant second-order transfer function model can be described by

$$P_{\text{PMLM}}(s) = \frac{k_1}{s(s^2 + a_1 s + a_2)} \tag{5}$$

where $k_1 = k_f/mL$, $a_1 = R/L$, and $a_2 = k_e k_f/mL$. This choice of model also greatly facilitates the use of automatic control tuning approaches [5].

B. PWM Amplifier

The recent availability of high-voltage and high-current PWM amplifiers in hybrid packages has attracted the interest of many servo drive designers who traditionally use linear amplifiers. The main advantage of PWM amplifiers over linear amplifiers is clearly in the power transfer efficiency. An efficiency of 70% to 90% can readily be achieved with PWM amplifiers. High efficiency also translates into lower internal power loss, smaller heat sinks, and therefore a reduced overall physical size. One can also use PWM amplifiers to emulate linear constant-voltage amplifiers or linear constant-current amplifiers, both at much higher levels of efficiency compared to linear amplifiers.

The PWM amplifier concerned here is a sinusoidal PWM with bipolar switching and it uses a triangular carrier. This PWM amplifier converts a sinusoidal signal (which may be from the output of a dc–ac converter) into a pulse train of variable duty

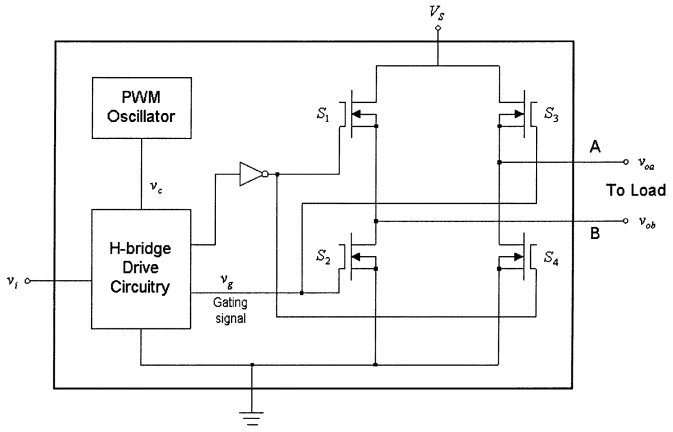

Fig. 2. Basic structure of a PWM amplifier.

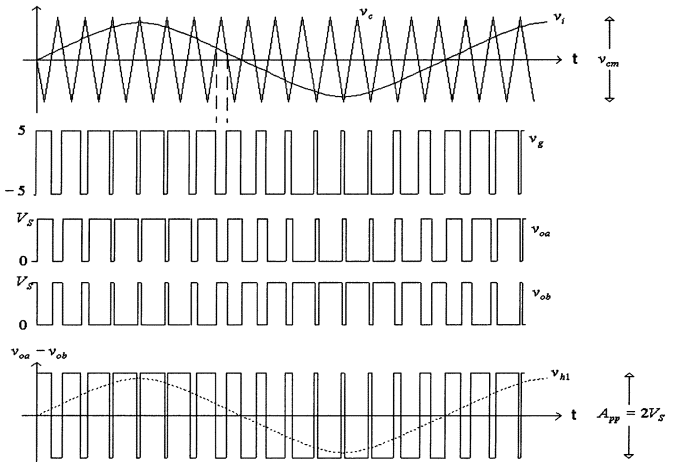

Fig. 3. Pulsewidth-modulated signal.

cycle. The PWM input controls the duty cycle of the output pulse train, which switches on and off once during each cycle. When a high output is required, the pulse train will have a duty cycle that approaches 100%. Fig. 2 shows the basic structure of a PWM amplifier. v_i is the analog input to be modulated; whereas v_{oa} is a pulse train and v_{ob} is its inverse. The PWM oscillator provides the switching frequency (or carrier frequency). The bridge drive circuitry thus consists of a comparator which compares the input signal v_i and the triangular carrier v_c to generate a sequence of pulses to trigger the H-bridge as depicted in Fig. 3. The switching moments are determined by the crossover points of the two waveforms.

The metal–oxide–semiconductor field-effect transistors (MOSFETs) of the H-bridge (S_1, S_2, S_3 and S_4) simply act as switches. The gating signal (TTL), v_g turns the MOSFETs on and off in diagonal sets, i.e., when S_1 and S_4 are on, S_2 and S_3 are off, and vice versa. As v_i changes from its minimum to its maximum, the duty cycle of v_{oa} changes from 0 to 100% and from its inverse v_{ob} changes from 100% to 0, and vice versa. The differential voltage $v_{oa} - v_{ob}$ has the same waveform as the pulse train v_{oa}, but it has the amplitude of the motor rated voltage. This simple voltage amplification feature is another advantage PWM amplifiers offer for high-voltage applications over the linear amplifiers.

The pulse trains at outports *A* and *B* can be connected directly to a motor because the motor, which is essentially a low-pass filter, would screen out the high harmonics of the pulsed voltage and hence produce an analog signal. It is, however, advisable to connect inductance–capacitance (LC) filters next to the amplifier module or to have built-in LC filters. The filters are useful for electromagnetic interference (EMI) cancellation and electromagnetic compatibility (EMC) purposes. Without the filters, the long cables to the motor carry high-voltage switching pulses and acts as antennas. If an external filter is required, a rule of thumb is to set the corner frequency (or cutoff frequency) of the LC filter to be one decade below the PWM switching frequency.

In our testbed system, the linear actuator is driven by a sinusoidal PWM amplifier (bipolar switching) with a triangular carrier of 20 kHz. In our previous works ([6], [7]), we have observed that the harmonic frequency contents in the PWM output are not negligible [11], and they can adversely affect positioning accuracy. In many motion control systems where the control performance requirements are modest, the dynamics of the PWM amplifier are simply ignored and only the PMLM is modeled. However, when the performance requirements become more stringent, it is necessary to explicitly account for the dynamics associated with the PWM amplifier. In this paper, we will derive a model for the PWM amplifier based on a describing function approach [8]. Based on the overall model, consisting of the PWM amplifier and the PMLM, the controller will be designed.

As in a typical describing function analysis, we assume a sinusoidal input to the PWM amplifier, given by

$$v_i(t) = v_{im}\cos(\omega t). \tag{6}$$

This is also a natural input to the PWM amplifier, since the usual dc input from the controller will be converted into a sinusoid of an appropriate frequency via a dc–ac converter. The PWM output will consist of a sequence of pulses at the fundamental frequency of ω (Fig. 4). Using Fourier analysis, this periodic signal can be equivalently decomposed into a fundamental sinusoid and its high frequency harmonics, i.e.,

$$v_o(t) = \sum_{i=1}^{\infty} v_{hi}\cos(i\omega t + \varphi_i) \tag{7}$$

where v_{hi} is the Fourier coefficient corresponding to the ith harmonic.

If we assume that the higher harmonics will be naturally filtered via the low-pass characteristics of the PMLM (filtering hypothesis), we may consider only the fundamental frequency, i.e., $v_o(t) = v_{h1}\cos(\omega t + \varphi_1)$.

The approximate frequency response of the PWM amplifier is thus given by [8]

$$|G(j\omega)| = \frac{v_{h1}}{v_{im}} \tag{8}$$

$$\arg[G(j\omega)] = \varphi_1. \tag{9}$$

We may assume that the gain is linear so that

$$\frac{v_{h1}}{v_{im}} = \frac{A_{pp}}{v_{cm}}.$$

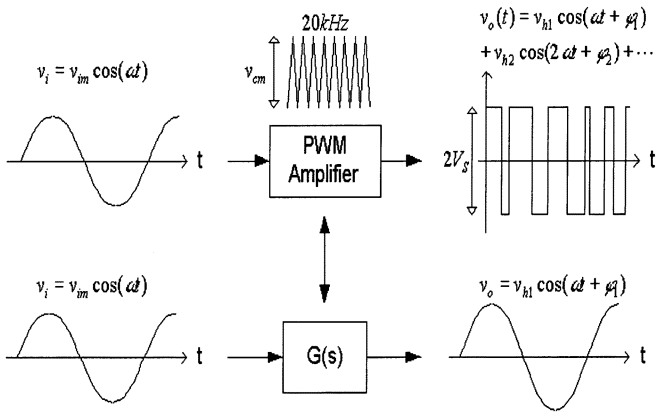

Fig. 4. Describing function analysis of the PWM amplifier.

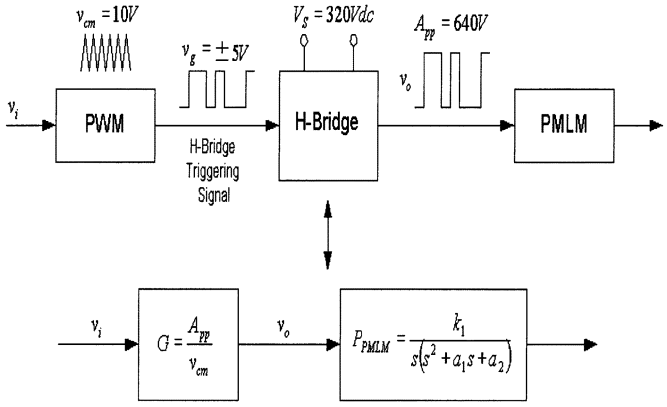

Fig. 5. Overall model.

The frequency response can be converted to a parametric transfer function with a delay (φ_1/ω)

$$G(s) = \frac{A_{pp}}{v_{cm}} e^{-s(\varphi_1/\omega)}. \tag{10}$$

Usually, φ_1 is small so that the delay term may be ignored.

C. Overall Model

Fig. 5 shows the schematic diagram of the overall model of a PMLM driven by a PWM amplifier. The PWM amplifier is described by a constant gain whereas the PMLM is represented by a third-order transfer function. The PWM amplifier acts as a pulse generator. The gating signal generated, v_g, will trigger the H-bridge to give an amplified pulsating signal. The output of the power electronics circuit, v_o, is finally filtered to produce an analog signal that is in turn used to drive the PMLM.

III. Design of the Disturbance Observer

In this section, a robust control scheme employing a disturbance observer [12] is proposed to reduce the sensitivity of the control performance to disturbances, more notably in the form of high harmonics from PWM amplifiers, ripple forces, and load changes. Fig. 6 shows the block diagram of the proposed control system which uses an estimate of the actual disturbance, deduced from a disturbance observer, to compensate for the disturbances. r, u, ξ, y, d, and $\hat{d}$ denote the reference signal, control signal, measurement noise, system output, actual and estimated disturbance, respectively. The disturbance observer, shown demarcated within the dotted box in Fig. 6, estimates the disturbance based on the output x and the control signal u. P denotes the actual system. P_n denotes the nominal system, which can be generally described by

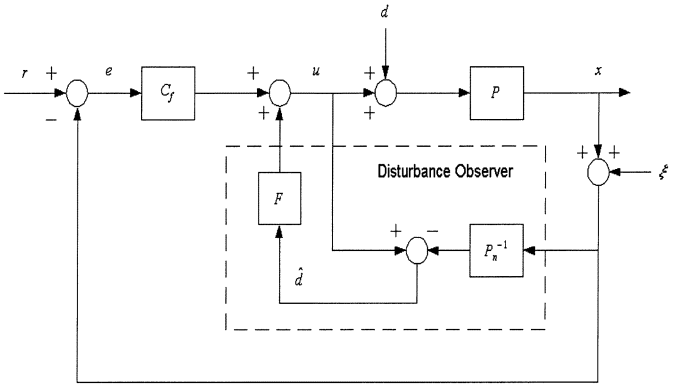

Fig. 6. Control system with disturbance observer.

$$P_n = \frac{1}{s^l(s^{m-l} + a_1 s^{m-l-1} + \cdots + a_{m-l-1}s + a_{m-l})} \tag{11}$$

where P_n is a mth order delay system and has l poles at the origin. In this paper, as mentioned, we will use a third-order model, i.e., $l = 1$, $m = 3$

$$P_n = \frac{1}{s(s^2 + a_1 s + a_2)}. \tag{12}$$

The disturbance observer incorporates the inverse of the nominal system, and thus a low-pass filter F is required to make the disturbance observer proper and practically realizable. For our choice of a third-order model P_n, a suitable filter is

$$F(s) = \frac{f_3}{s^3 + f_1 s^2 + f_2 s + f_3}. \tag{13}$$

Higher order filters may be used which can predict the occurrence of the disturbances earlier. C_f is the feedback controller that is usually designed with respect to the nominal system P_n. The estimated disturbance is added to the overall input to cancel the effects of the disturbances. Thus, this function is similar to a feedforward compensator, and it can improve the transient performance to the disturbance as well as the steady-state operations.

Within the bandwidth of the observer filter F, the control system with the disturbance observer as depicted in Fig. 6 essentially approximates a nominal system without disturbances. This observation may be clearer by transforming Fig. 6 to the equivalent configuration of a filter-type two-degree-of-freedom control system, as depicted in Fig. 7. Fig. 7 shows that the disturbance observer is equivalent to an additional disturbance compensator C_{obsv}, which closes a fast inner loop [9]. Consequently, we can consider that the thus compensated inner loop constitutes essentially a nominal system without disturbances, since they have been compensated by C_{obsv}.

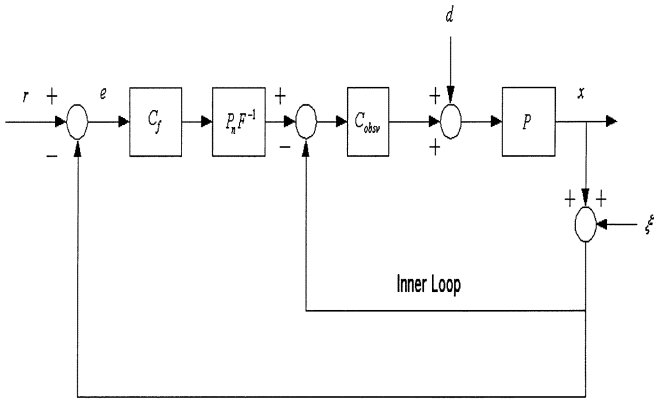

Fig. 7. Equivalent system to Fig. 6.

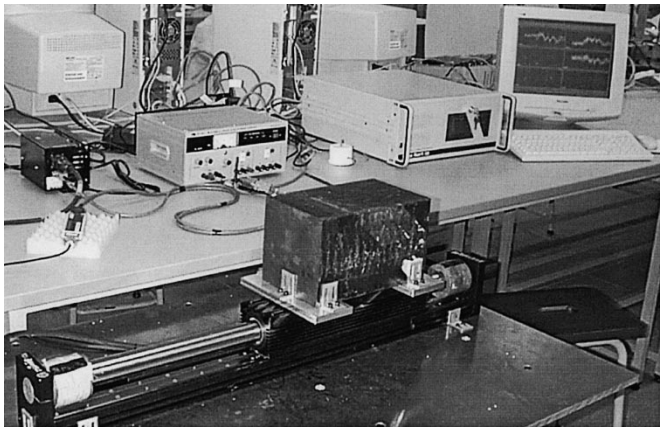

Fig. 8. Setup of the laboratory testbed.

It can be shown that

$$C_{\text{obsv}} = \frac{F}{1-F} P_n^{-1}. \tag{14}$$

For our choice of P_n and F, we thus have

$$C_{\text{obsv}} = \frac{f_3(s^2 + a_1 s + a_2)}{s^2 + f_1 s + f_2}. \tag{15}$$

Therefore, C_{obsv} can be considered as a lead/lag compensator by appropriately designing f_1, f_2, and f_3 relatively to a_1 and a_2.

The disturbance observer can be designed in many ways. In this paper, it is proposed that it be designed as follows.

- Identify the nominal model (i.e., a_1, a_2), based on which the outer loop controller C_f can be designed to achieve a desired command response. If C_f is a PID controller, many design methods are available ([6] and [14]).
- Adjust f_1, f_2, and f_3 of the disturbance compensator C_{obsv} to satisfy requirements for robustness and disturbance suppression characteristics. The system sensitivity function and the system transmission function can thus be set independently. Such a feature is especially useful when there are strict requirements on both setpoint tracking and disturbance suppression and an acceptable compromise between these sometimes conflicting requirements might not exist.
- Carry out simulation and fine tuning until the performance is acceptable.

IV. Experimental Results

In the experimental studies, an industrial grade PMLM, manufactured by Linear Drives U.K., is used. This is a direct thrust tubular motor (LD 3810) driven by a PWM amplifier with a triangular carrier of 20 kHz. The only transducer equipped in the testbed system is a Renishaw optical encoder with an effective resolution of 1 μm. The experimental setup is as shown in Fig. 8.

The control algorithms are implemented on DS1102 DSP Controller Board from dSPACE GmbH, which utilizes TI's TMS320C31 32-bit floating point processor with 60 MHz of execution frequency. Control algorithms are implemented simply via Simulink block diagrams with MATLAB RTI (real-time interface), compiled on an IBM personal computer (PC) which can be downloaded into the DS1102 board. The dSPACE control development and rapid prototyping system integrate the entire development cycle seamlessly into a single environment, so that individual development stages between simulations and tests can be run and rerun without frequent readjustment.

Throughout the experimental studies, the trajectory profile is prescribed as

$$x_d(\tau) = 10^6[x_0 + (x_0 - x_f)(15\tau^4 - 6\tau^5 - 10\tau^3)] \tag{16}$$

where 10^6 is used to normalize the system units to microns. x_d and $\dot{x}_d$ denote the desired position and velocity trajectories; x_0 and x_f denote the initial and final positions which are assigned to be 0 and 21 000 μm (i.e., 210 mm), respectively. $\tau = t/(t_f - t_0)$, where t_0 and t_f are the initial time and final time of the trajectory.

Substituting the various constants associated with the manufacturer specifications into (5) yields a dominant model of PMLM as

$$P_{\text{PMLM}} = \frac{1245}{s(s^2 + 970.8s + 1.53 \times 10^5)}. \tag{17}$$

The PWM amplifier has a triangular carrier with peak-to-peak amplitude of 10 V and the PWM output ranges from -5 to $+5$ V. The pulses trigger the bridge circuit to give an amplified pulsating voltage ranging from -320 to 320 V, which is then used to drive the PMLM. The overall amplifier gain is thus given by

$$G = \frac{2 \times 320}{10} = 64. \tag{18}$$

Normalizing to microns, the overall dominant model can be written as

$$P_n = \frac{7.75 \times 10^{10}}{s(s^2 + 970.8s + 1.53 \times 10^5)}. \tag{19}$$

The real-time experimental results obtained, as given in Fig. 9, show that the controller with disturbance observer can achieve a tracking error of less than 7 μm. The controller performs satisfactorily even when a load disturbance is deliberately introduced

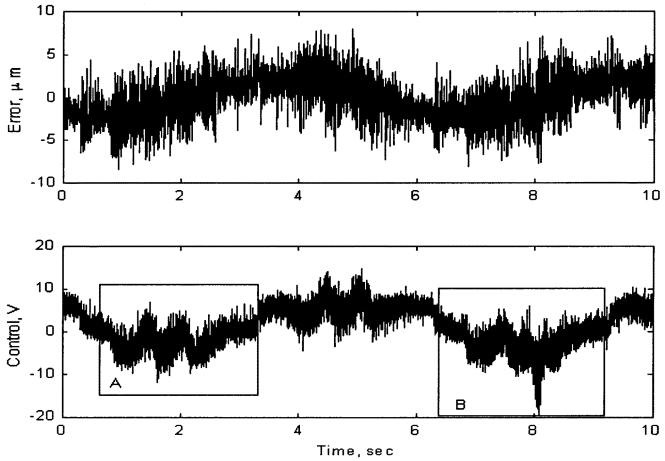

Fig. 9. Experimental results with disturbance observer.

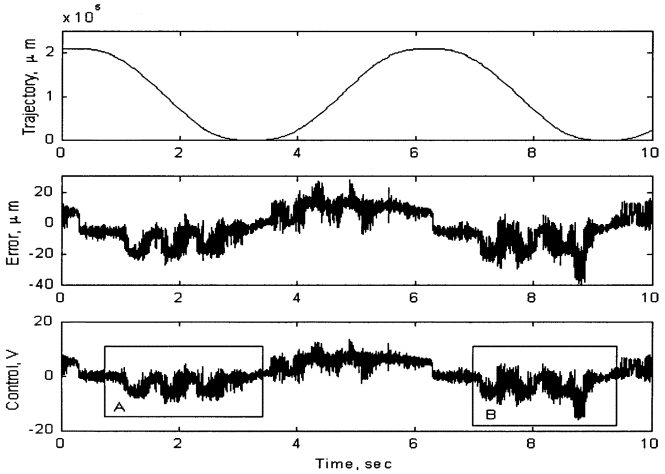

Fig. 10. Experimental results without disturbance observer: (a) desired trajectory (μm); (b) error (μm); (c) control signal (V).

into the system (*Box B* in Fig. 9). For comparison, *Box A* highlights the performance of the system before the introduction of the load disturbance. The changes in control signal due to the introduction of disturbance are not reflected in the error signal. In other words, the control system is able to reject the external disturbance and the performance is not affected.

To further illustrate the performance enhancement from the use of the disturbance observer, control results without the observer are shown in Fig. 10. The deliberate load disturbance introduced into the system is clearly manifested in the error signal (*Box B* in Fig. 10). A comparison between Figs. 9 and 10 shows that the use of the disturbance observer is not only effective in reducing the tracking error, but also useful in eliminating or reducing the inherent force ripple that is characterized by a w-shaped signal in the control signal.

V. Conclusion

This paper has addressed the development of a PMLM motion controller with a disturbance observer to achieve enhanced control performance when significant amount of disturbances is present. A mathematical overall model of the PMLM and the sinusoidal PWM amplifier is first established. Based on this model, a robust control scheme employing the disturbance observer has been developed to reduce the sensitivity of the control performance to disturbances. Real-time experimental results have verified and confirmed the practical effectiveness of the proposed approach. The proposed control system yields a much more superior performance compared to one without the observer.

References

[1] A. Basak, *Permanent-Magnet DC Linear Motors, Monographs in Electrical and Electronic Engineering*. Oxford, U.K.: Clarendon, 1996.

[2] B. Yao and L. Xu, "Adaptive robust control of linear motors for precision manufacturing," in *Proc. 14th Triennial World Congr.*, Beijing, China, 1999, pp. 25–30.

[3] G. Otten, T. J. A. de Vries, J. van Amerongen, A. M. Rankers, and E. W. Gaal, "Linear motor motion control using a learning feedforward controller," *IEEE/ASME Trans. Mechatron.*, vol. 2, pp. 161–170, Sept. 1997.

[4] S. Chang, S. H. Wu, and Y. Hu, "Submicrometer overshoot control of rapid and precise positioning," *J. Amer. Soc. Precision Eng.*, vol. 20, pp. 161–170, 1997.

[5] K. K. Tan, H. F. Dou, Y. Q. Chen, and T. H. Lee, "High precision linear motor control via artificial relay tuning and zero-phase filtering based iterative learning," *IEEE Trans. Control Syst. Technol.*, vol. 9, pp. 244–253, Mar. 2001.

[6] K. K. Tan, S. N. Huang, H. F. Dou, S. Y. Lim, and S. J. Chin, "Adaptive robust motion control for precise trajectory tracking applications," *ISA Trans.*, vol. 40, no. 1, pp. 57–71, 2001.

[7] K. K. Tan and S. J. Chin, "Ripple suppression in precision production systems using a simplex approach," in *Int. Conf. Production Research*, Bangkok, Thailand, 2000.

[8] P. P. Robet, M. Gautier, and C. Bergmann, "A frequency approach for current loop modeling with a PWM converter," *IEEE Trans. Indust. Applicat.*, vol. 34, pp. 1000–1014, Sept./Oct. 1998.

[9] K. Yamada, S. Komada, M. Ishida, and T. Hori, "Analysis of servo system realized by disturbance observer," *Proc. IEEE Int. Workshop Advanced Motion Control*, pp. 338–343, 1996.

[10] K. K. Tan, T. H. Lee, S. Y. Lim, and H. F. Dou, "Learning enhanced motion control of permanent magnet linear motor," in *Proc. 3rd IFAC Int. Workshop Motion Control*, Grenoble, France, 1998, pp. 397–402.

[11] R. Tymerski, V. Vorperian, F. C. Y. Lee, and W. T. Baumann, "Nonlinear modeling of the PWM switch," *IEEE Trans. Power Electron.*, vol. 4, pp. 225–233, April 1989.

[12] K. Yamada, S. Komada, M. Ishida, and T. Hori, "Analysis and classical control design of servo system using high order disturbance observer," in *23rd Int. Conf. Industrial Electronics, Control and Instrumentation IECON 97*, vol. 1, 1997, pp. 4–9.

[13] W. L. Luyben, *Process Modeling, Simulations and Control for Chemical Engineers*. New York: McGraw-Hill, 1990.

[14] P. Dorato, C. Abdallah, and V. Cerone, *Linear-Quadratic Control: An Introduction*. Englewood Cliffs, NJ: Prentice-Hall, 1995.